AIAA JOURNAL
Vol. 30, No. 3, March 1992

Boundary Element Method for the Analysis of the Unsteady Flow Around Extreme Propeller Geometries

Spyros A. Kinnas* and Ching-Yeh Hsin†
Massachusetts Institute of Technology, Cambridge, Massachusetts 02139

The unsteady flow around a marine propeller subject to a spatially nonuniform inflow is analysed by utilizing a time-marching potential-based low-order boundary element method. Constant strength dipole or source distributions are used on each of the quadrilateral panels representing the propeller blades and their trailing wakes. Linear dipole distributions are used at the first wake panels adjacent to the blade trailing edge in order to render the method insensitive to the time step size. An efficient algorithm is implemented in order to ensure an explicit Kutta condition (i.e., pressure equality) at the blade trailing edge at each time step. The numerical method is shown to be consistent with known analytic solutions for two-dimensional unsteady flows. The robustness of the method is tested in the case of a highly skewed propeller in a given wake inflow and the results are shown to converge quickly with number of panels for a broad range of reduced frequencies.

I. Introduction

MARINE propellers are very often subject to severe nonaxisymmetric wakes produced from the boundary layer of the vehicle. In the process of determining the complete propeller/wake interaction, one important step is the analysis of the unsteady potential flow around a propeller in the presence of a prescribed spatially nonuniform inflow. Accurate predictions of the unsteady pressure distributions on the blade, especially at the blade leading edge and tip, are crucial in determining cavitation inception, unsteady boundary-layer separation, as well as leading-edge vortex separation. Therefore, numerical methods for predicting the unsteady pressure distributions on the propeller blades must be computationally robust and reliable at all frequencies of the incoming flow, especially when applied to extreme propeller geometries (high skew and/or high twist) which in recent years have become very common.

Numerical lifting surface methods have been extensively applied for the analysis of unsteady propeller flows. One of the first investigators to formulate the unsteady propeller lifting surface problem in terms of the acceleration potential was Hanaoka.[1,2] The acceleration potential formulation was implemented, in terms of finite number of chordwise modes, by Tsakonas et al.[3,4] More recently, the unsteady vortex lattice technique was employed by Kerwin and Lee.[5] A review of the different steady and unsteady lifting surface methods as applied to marine propellers has been given by Kerwin.[6]

One of the major drawbacks of the lifting surface methods though is their inherent failure at the blade leading edge and tip where the blade thickness effects are substantial. On the other hand, boundary element or panel methods (BEMs) have been applied for the analysis of the steady flow around marine propellers, including the hub by, among others, Hess and Valarezo,[7] Kerwin et al.[8] (who also included the duct), and Hoshino.[9] The first of those methods employs a source-based formulation,[10] and the other two employ a potential-based formulation.[11]

BEMs were first extended to treat unsteady flows around two-dimensional hydrofoils by Giesing,[12] who employed a source-based formulation, and then by Basu and Hancock[13] who employed a surface vorticity formulation but also allowed for wake relaxation. More recently, BEMs have been extended to treat the unsteady flow around helicopter blades by Maskew[14] and by Morino et al.,[15] with emphasis given to the evolution of the rotor free wakes.

In the present work, a time-marching potential-based boundary element method is developed for the analysis of the unsteady flow around extreme propeller geometries, with emphasis on the accurate prediction of unsteady blade pressures and forces for a broad range of reduced frequencies. A computationally efficient explicit Kutta condition is implemented in the BEM in order to ensure pressure equality at the blade trailing edge at each time step. The numerics of the present method are tested for a highly skewed propeller in unsteady flow and are shown to be robust with respect to the size of the time step and the number of panels on the blade for a broad range of reduced frequencies. The numerical method is also shown to be consistent with existing analytic solutions for unsteady flows in two dimensions.

II. Formulation

Consider a propeller subject to a spatially nonuniform inflow $U_S(x_S, r_S, \theta_S)$, as shown in Fig. 1. The inflow is taken with respect to the absolute (ship fixed) system of cylindrical coordinates x_S, r_S, θ_S. The flow around the propeller will be analyzed with respect to the propeller fixed system (x, y, z), also shown in Fig. 1. If the propeller rotates with angular velocity $-\omega$ (i.e., right-handed propeller), then the inflow

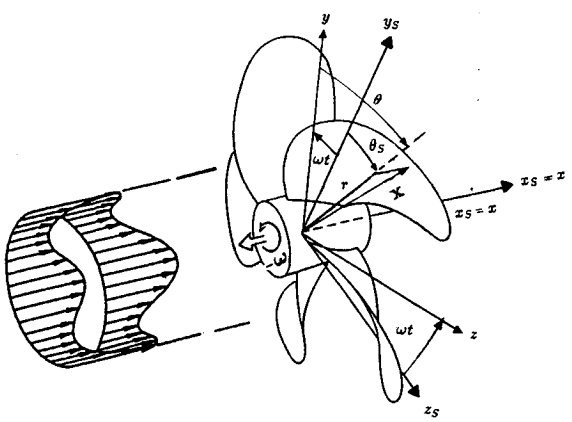

Fig. 1 The propeller in a spatially nonuniform inflow.

Received Dec. 10, 1990; revision received June 20, 1991; accepted for publication June 27, 1991.

*Research Engineer and Lecturer, Department of Ocean Engineering, MIT Rm. 5-221, 77 Massachusetts Ave.

†Postdoctoral Associate, Department of Ocean Engineering, MIT Rm. 5-028, 77 Massachusetts Ave.

relative to the propeller, U_{in}, will be time dependent and given as

$$U_{in}(x, y, z, t) = U_S(x, r, \theta - \omega t) + \omega \times x \qquad (1)$$

where $r = \sqrt{y^2 + z^2}$, $\theta = \arctan(z/y)$, and $x = (x, y, z)$.

We assume at this point, that the flow is incompressible and inviscid. In addition, the inflow U_S is assumed to be the effective wake, which includes the interactions between the vorticity of the inflow in the absence of the propeller (nominal wake) and the vorticity due to the propeller. Then, the time-dependent total flow velocity relative to the propeller fixed system, $q(x, y, z, t)$, can be written in terms of the perturbation potential, $\phi(x, y, z, t)$, as follows:

$$q(x, y, z, t) = U_{in}(x, y, z, t) + \nabla\phi(x, y, z, t) \qquad (2)$$

By applying Green's formula for $\phi(x, y, z, t)$ at any time t, we will get the following integral equation for the perturbation potential ϕ_p at every point p on the propeller blade surface S_P:

$$2\pi\phi_p = \int_{S_P} \left[\phi_q \frac{\partial G(p; q)}{\partial n_q} - G(p; q) \frac{\partial \phi_q}{\partial n_q} \right] dS + \int_{S_W} \Delta\phi(r_q, \theta_q, t) \frac{\partial G(p; q)}{\partial n_q} dS \qquad (3)$$

with the subscript q corresponding to the variable point in the integrations; n_q is the unit vector normal to the propeller surface or to the wake surface, $\Delta\phi$ is the potential jump across the wake sheet, and $G(p; q)$ is the Green's function. In the case of unbounded three-dimensional fluid domain $G(p; q) = 1/R(p; q)$, with $R(p; q)$ being the distance between points p and q.

Equation (3) expresses the potential on the propeller blade as the superposition of the potentials induced by a continuous source distribution, G, on the propeller surface, S_P, and a continuous dipole distribution, $\partial G/\partial n$, on the propeller surface S_P and its wake S_W. The strength of the source distribution is given, via the kinematic boundary condition, as

$$\frac{\partial \phi_q}{\partial n_q} = -U_{in}(x_q, y_q, z_q, t) \cdot n_q \qquad (4)$$

where x_q, y_q, z_q are the coordinates of point q with respect to the propeller fixed system.

The strength of the dipole distribution is unknown and equal to the perturbation potential on the propeller or to the potential jump in the wake. The dipole strengths will be determined by inverting integral Eq. (3). The trailing wake, S_W, is assumed to be invariant with time and taken to be the same as the steady-flow relaxed wake corresponding to the circumferentially averaged inflow.[16] The dipole strength $\Delta\phi(r, \theta, t)$ in the wake is convected along the assumed wake model with angular speed ω, in order to ensure that the pressure jump in the wake is equal to zero, i.e.,

$$\Delta\phi(r, \theta, t) = \Delta\phi_T\left(r, t - \frac{\theta - \theta_T(r)}{\omega}\right); \; t \geq \frac{\theta - \theta_T(r)}{\omega}$$

$$\Delta\phi(r, \theta, t) = \Delta\phi^S(r); \; t < \frac{\theta - \theta_T(r)}{\omega} \qquad (5)$$

where r, θ are the cylindrical coordinates of the wake surface, S_W, and $\theta_T(r)$ is the θ coordinate of the propeller blade trailing edge at radius r. $\Delta\phi^S(r)$ is the steady flow potential jump in the wake when the propeller is subject to the circumferentially averaged inflow. For $t < 0$ we assume that the propeller is subject to the circumferentially averaged inflow. The unsteady inflow is "turned on" at $t = 0$.

The value of the dipole strength, $\Delta\phi_T(r, t)$, at the trailing edge of the blade at time t, will be given by

$$\Delta\phi_T(r, t) = \phi_T^+(r, t) - \phi_T^-(r, t) = \Gamma(r, t) \qquad (6)$$

where $\phi_T^+(r, t)$ and $\phi_T^-(r, t)$ are the values of the potential at the upper (suction side) and lower (pressure side) blade trailing edge, respectively, at time t. The difference in those potentials is also equal to the circulation Γ at time t around the blade section at radius r. The condition [Eq. (6)] is equivalent to requiring the shed vorticity from the blade trailing edge to be proportional to the time rate of change of the circulation around the blade.

III. Numerical Implementation

Equation (3) is a Fredholm integral equation of the second kind with respect to ϕ_p. To solve this equation numerically, we discretize the propeller and wake surface into quadrilateral panels. A typical panel arrangement for a propeller and its wake is shown in Fig. 2. Only the transition trailing wake is shown in Fig. 2. The ultimate wake geometry is represented with an actuator disk at the end of the transition wake as described in Ref. 17. The propeller blade panel arrangement is identical to that used in the propeller steady-flow BEM.[17] The time domain is also discretized into equal time intervals Δt. The panels in the wake start from the blade trailing edge and their edges are located on the prescribed wake surface at equal angular spacing $\Delta\theta_W$, which is related to the time step Δt as follows:

$$\Delta\theta_W = \omega\Delta t \qquad (7)$$

On each of the quadrilateral panels, the dipole or source distributions are approximated by constant strength distributions. The discretized version of the integral Eq. (3) is applied at the centroids of each of the propeller panels and at each time step $n = t/\Delta t$. This renders the following system of linear equations:

$$\sum_{K=1}^{N_B} \sum_{j=1}^{N_P} a_{i,j}^K \phi_j^K(n) + \sum_{K=1}^{N_B} \sum_{m=1}^{M} \sum_{l=1}^{N_W} W_{i,m,l}^K \Delta\phi_{m,l}^K(n) = \sum_{K=1}^{N_B} \sum_{j=1}^{N_P} b_{i,j}^K \sigma_j^K(n); \quad i = 1, N_P \times N_B \qquad (8)$$

where N_B is the number of blades, and for each blade, N is the number of chordwise panels, M is the number of spanwise panels, $N_P = N \times M$ is the total number of panels, and N_W is the number of panels in the wake along the streamwise direction, as shown in Fig. 2.

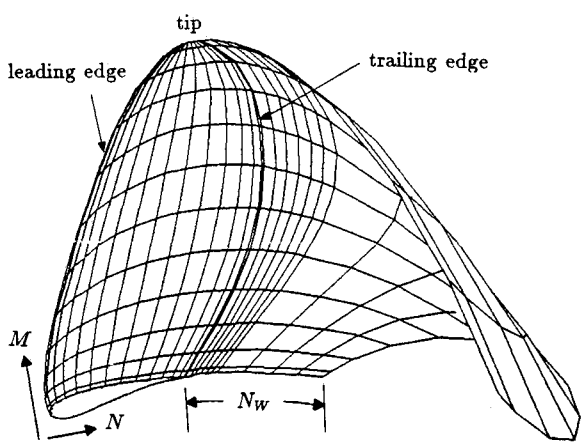

Fig. 2 Panel arrangement for a propeller blade and its wake, N = 20, M = 10, $\Delta\theta_W$ = 6 deg.

The influence coefficients $a_{i,j}^K$ and $b_{i,j}^K$ are defined as the potentials induced at panel i by unit (constant) strength dipole and source distributions, respectively, located at panel j on blade K. The wake influence coefficients $W_{i,m,l}^K$ are defined similarly. The shape of the surface bounded by the edges of each panel (nonplanar in general) is approximated by a hyperboloidal surface, and the corresponding influence coefficients are evaluated by using analytical expressions.[11,18,19] The use of hyperboloidal surface panels instead of planar panels has been found to be crucial for the consistency and convergence of the steady flow propeller BEM, especially when applied to extreme propeller geometries (i.e., high skew and twist).[19] A similar conclusion has also been reached by Hoshino.[9]

The source strength $\sigma_j^K(n)$ is defined from Eq. (4) as

$$\sigma_j^K(n) = -\boldsymbol{U}_{in}(x_j^K, y_j^K, z_j^K, n\Delta t) \cdot \boldsymbol{n}_j^K \tag{9}$$

with x_j^K, y_j^K, z_j^K being the coordinates of the centroid of panel j on blade K and $\boldsymbol{n}_j^K$ being the unit vector normal to that panel.

The terms in Eq. (8) can be regrouped as (the superscript 1, which denotes the key blade, is omitted):

$$\sum_{j=1}^{NP} a_{i,j}\phi_j(n) + \sum_{m=1}^{M} W_{i,m,1}\Delta\phi_{m,1}(n) = RHS_i(n)$$

$$i = 1, N_P \tag{10}$$

where

$$RHS_i(n) = \sum_{K=1}^{NB}\sum_{j=1}^{NP} b_{i,j}^K\sigma_j^K(n) - \sum_{K=2}^{NB}\sum_{j=1}^{NP} a_{i,j}^K\phi_j^K(n) - \sum_{K=2}^{NB}\sum_{m=1}^{M}\sum_{l=1}^{NW} W_{i,m,l}^K\Delta\phi_{m,l}^K(n) - \sum_{m=1}^{M}\sum_{l=2}^{NW} W_{i,m,l}\Delta\phi_{m,l}(n). \tag{11}$$

The system of equations (10) must be solved at each time step n with respect to the potentials on the key blade, $K = 1$. The potentials on the other blades ($K > 2$) and their wakes, which appear on the right-hand side of Eq. (10), are taken equal to those on the key blade at an earlier time step, when the blade K was at the place of the key blade. This scheme, already used in an unsteady propeller lifting surface vortex lattice method,[5] is essentially an iterative method for solving the system of equations (8) in order to determine the steady-state oscillatory solution for a given inflow. The solution, in most cases, was found to converge after three propeller revolutions. Solving Eq. (10) instead of Eq. (8) requires the inversion of a much smaller matrix and thus reduces substantially the computing time. It also requires less computer storage, since only the solution for the key blade, rather than for all blades, needs to be stored at each time step. The values of $\Delta\phi_{m,l}(n)$ for $l > 2$ (i.e., for all panels in the wake, except those next to the trailing edge) are determined from the discretized form of Eq. (5):

$$\Delta\phi_{m,l}(n) = \Delta\phi_{m,1}(n - l + 1);\ l \geq 2,\ n \geq l$$

$$\Delta\phi_{m,l}(n) = \Delta\phi_m^S;\ l \geq 2,\ n < l \tag{12}$$

On the other hand, the value of the potential $\Delta\phi_{m,1}$ at the first wake panel may be given, by using Eq. (6), as

$$\Delta\phi_{m,1} = \frac{\Gamma_m(n) + \Gamma_m(n-1)}{2} \tag{13}$$

with $\Gamma_m(n)$ denoting the circulation around the blade strip m at time step n. In deriving Eqs. (12) and (13), the continuous dipole distribution over each wake panel is approximated by a constant distribution with strength equal to the mean value of the potentials at the edges of the panel, as shown in Fig. 3. Numerically, $\Gamma_m(n)$ is approximated by

$$\Gamma_m(n) = \phi_m^+(n) - \phi_m^-(n) \tag{14}$$

where ϕ_m^+ and ϕ_m^- are the potentials at the upper and lower trailing-edge panel, respectively, at blade strip m. The right-hand side of Eq. (14) approximates the jump in the potential at the trailing edge by the difference between the potentials at the trailing-edge control points on the blade, as shown in Fig. 3. Equation (14) is an extension of Morino's Kutta condition in steady flow.[11] However, in the case of unsteady flow, Morino et al.[15] approximate the potential at the first wake panel, $\Delta\phi_{m,1}$, with the circulation at the previous time step, $\Gamma_m(n-1)$, instead of using Eq. (13). An improvement on Eq. (14) is presented in Sec. IV. By substituting Eqs. (14) and (13) into Eq. (10), a linear system of equations is derived with respect to the unknown potentials $\phi_j(n)$ on the key blade. This system of equations is inverted at each time step n.

A modification on this numerical scheme has been implemented, in which the dipole sheet on the first wake panel is approximated by a linear instead of a constant distribution. As is described in Sec. V.A, that modification is necessary to make the results of the unsteady BEM practically insensitive to the size of the time step. In that case, the system of equations (10) will be modified to be

$$\sum_{j=1}^{NP} a_{i,j}\phi_j(n) + \sum_{m=1}^{M} T_{i,m}^L\Gamma_m(n) = \overline{RHS}_i(n)$$

$$i = 1, N_P \tag{15}$$

with

$$\overline{RHS}_i(n) = RHS_i(n) - T_{i,m}^R\Gamma_m(n-1); \qquad i = 1, N_P \tag{16}$$

and where $T^L(T^R)$, as described in more detail in Appendix A, are the influence coefficients of a linear dipole distribution (in the chordwise direction) with unit value at the left (i.e., trailing edge) (right) edge and zero value at the right (left) edge. By substituting Eq. (14) in Eq. (15) we end up, at each time step, with a system of N_P linear equations with respect to the N_P unknown potentials on the panels of the key blade. Equation (15) can also be written in the following matrix form

$$[A][\phi] + [T][\Gamma] = [RHS] \tag{17}$$

with $[A]$, $[\phi]$, and $[T]$ being the matrices of $a_{i,j}$, $\phi_j(n)$, and $T_{i,m}^L$, respectively, and

$$[\Gamma] = [\Gamma_1(n), \ldots, \Gamma_M(n)]^T$$

$$[RHS] = [\overline{RHS}_1(n), \ldots, \overline{RHS}_{NP}(n)]^T \tag{18}$$

An accelerated iterative block matrix solver is used for inverting Eq. (17). The diagonal elements of this block matrix,

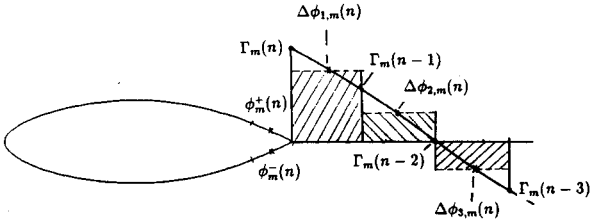

Fig. 3 Expanded view of the dipole distribution in the wake of blade strip m.

corresponding to each blade strip, are LU decomposed once and then used throughout the entire time-marching solution. The required CPU time on an IRIS 4D/25 TG in the case of a one-bladed propeller with $N = 40$, $M = 20$, and 240 total number of time steps (60 per revolution) is approximately 4 h.

IV. Unsteady Pressures and Kutta Condition

The pressure p at every point x on the blade and for each time step n is computed from the potentials on the blade by applying the unsteady-flow Bernoulli's equation with respect to the propeller system:

$$\frac{p}{\rho} + \frac{1}{2}q^2 + \frac{\partial \phi}{\partial t} = \frac{p_\infty}{\rho} + \frac{1}{2}q_\infty^2 \tag{19}$$

where ρ is the density of the fluid, q is the magnitude of the total surface velocity with respect to the propeller system at point x and time step n, p_∞ and q_∞ are the pressure and the magnitude of the velocity of the unperturbed flow, with respect to the propeller system, respectively. The surface velocity q is computed in terms of the derivatives of the perturbation potentials on the blade surface, in the same way as in the steady-flow BEM.[8] The $\partial\phi/\partial t$ term in Eq. (19) is computed numerically, by implementing a fourth-order-accurate backward finite difference scheme with respect to time. This scheme has been found to produce results that are less sensitive on the number of time steps per period of the inflow than an originally utilized second-order-accurate finite difference scheme.[19]

In the steady-flow BEM for propellers and ducts,[8] it was found that the numerical Kutta condition [Eq. (14)][11] was not sufficient and an iterative scheme was developed in order to modify the solution and ensure pressure equality at the trailing edge. An explicit pressure Kutta condition was also found to be required in the unsteady-flow BEM. For example, in Fig. 4 the unsteady pressure distributions before and after applying an explicit Kutta condition are shown for the OBO propeller and the wake inflow, both described in Sec. V.B. Notice the global effect of the explicit Kutta condition on the chordwise pressure distributions.

In order to ensure pressure equality at the blade trailing edge at each time step, the circulation around each strip is adjusted by implementing an iterative multidimensional Newton-Raphson scheme, the details of which are described in Appendix B. The effect of adjusting the circulation on the potential distribution of the propeller blades is determined in a computationally efficient manner in terms of the base problems, defined in Appendix B. The inviscid unsteady forces acting on each propeller blade are computed by integrating the unsteady pressure distributions on the surface of the blade, via a piecewise constant integration scheme over each panel.

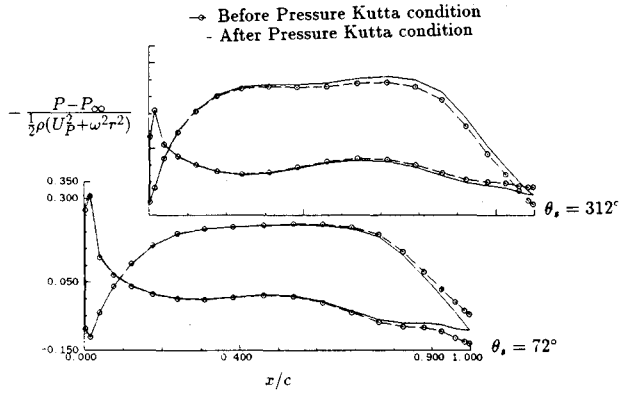

Fig. 4 Unsteady pressure distributions on the blade vs chordwise location at $r/R = 0.75$, before and after applying an iterative pressure Kutta condition, for the OBO propeller at blade angle $\theta_S = 72$ deg and $\theta_S = 312$ deg.

V. Numerical Validation of Unsteady-Flow BEM

In this section, the convergence of the results from the present unsteady-flow BEM when applied to two-dimensional geometries as well as to a highly skewed propeller is investigated by varying the principal discretization parameters. In addition, the consistency of the results from the present BEM with the analytical results for a flat plate in a sinusoidal gust is investigated.

A. Sinusoidal Gust in Two Dimensions

The two-dimensional version of the present method is applied to several symmetric modified NACA66 forms[20] with chord $c = 1$ and various maximum thicknesses, τ_{max}. The foils are subject to a sinusoidal gust normal to their chord, of amplitude $\tilde{v}_g = 0.2$ and frequency ω. The gust is carried downstream by a uniform flow $U = 1$ and reaches the leading edge of the foil at time $t = 0$, as shown in Fig. 5. The vorticity shed from the foil is positioned along the trailing-edge bisector line. The reduced frequency of the gust is defined as usual as

$$k = \frac{\omega c}{2U} \tag{20}$$

First, the sensitivity of the method to the size of the time step, Δt, is investigated, when a constant-strength dipole distribution is utilized in the first wake panel. The results, shown in Fig. 6, appear to be very dependent on the ratio of the length of the first wake panel $U\Delta t$ to the length of the trailing-edge panel Δx_T. Dependency on the time step is a very undesirable characteristic of any unsteady-flow BEM, especially if the method is expected to be able to handle low- as well as high-frequency components of the incoming flow.

However, when the first panel in the wake is represented by a linear rather than constant dipole distribution, as described in Sec. III, the results, shown in Fig. 7, become independent of the time step. Replacing the rest of the constant-strength panels in the wake with linear distribution was found to have no significant effect on the results. The poor performance of the constant-wake dipole panel is attributed to the fact that the potentials induced on the trailing-edge panels by the saw-tooth dipole distribution on the first wake panel, shown shaded in Figure 5, are not negligible. Those saw-tooth

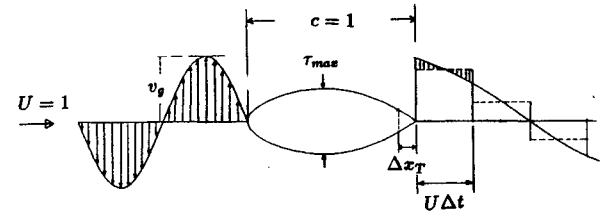

Fig. 5 Two-dimensional symmetric foil subject to a sinusoidal gust.

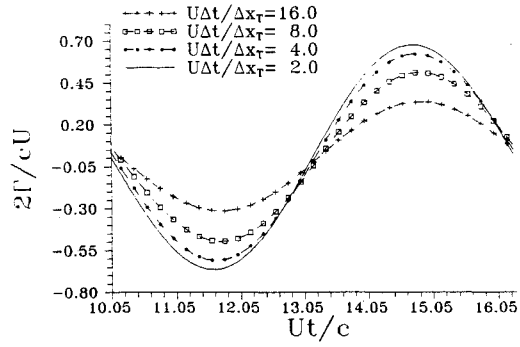

Fig. 6 Convergence of present BEM with time step size. Constant dipole distribution on the first wake panel. Modified NACA66 form, $\tau_{max}/c = 0.1$, $\tilde{v}_g = 0.2$, $k = 0.5$. Number of panels on the foil $N = 40$.

induced potentials become larger the larger the time step the slope of the dipole distribution at the trailing edge (i.e., frequency) are. As a result of the previous investigation, a linear dipole distribution is always employed in the first wake panel in the unsteady-flow BEM for hydrofoils as well as propellers. The convergence with number of panels on the foil, described in detail in Ref. 21, has been found to be very good for a broad range of reduced frequencies.

A direct comparison of the previously presented results with the analytical results for a flat plate in a sinusoidal gust, the well-known Sears problem,[22] is not possible. This is due to the fact that potential-based BEMs cannot treat zero-thickness hydrofoils since Eq. (3) degenerates to an identity for zero thickness, thus rendering a singular matrix in the numerical formulation. The consistency of the results from the BEM against the flat plate results, though, can be investigated by applying the BEM to a series of symmetric foils with various maximum thickness/chord ratios (maintaining the same thickness form) and by extrapolating the results to zero thickness. This is a special application of the consistency test of BEMs vs lifting surface (zero thickness) methods for wings and propellers, proposed by Kinnas.[21,23] The unsteady BEM is applied to three foils with τ_{max} = 0.05, 0.1, and 0.2. The results (in this case the time history of the circulation around the foil) appear to be linear in thickness and, thus, are linearly extrapolated to zero thickness and compared against the steady-state analytic circulation of a flat plate in a gust. The comparison is shown in Fig. 8 for a relatively high (k = 10) reduced frequency. The consistency test appears to be valid, within acceptable accuracy.

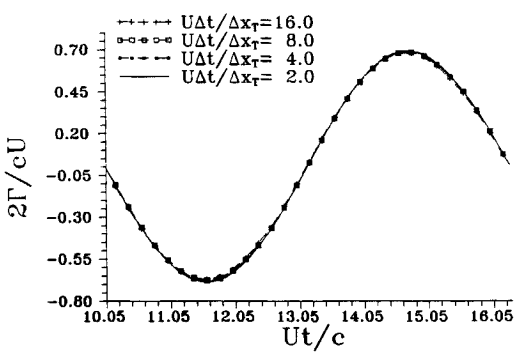

Fig. 7 Convergence of present BEM with time step size. Linear dipole distribution on the first wake panel. Same geometry and flow conditions as in Fig. 6.

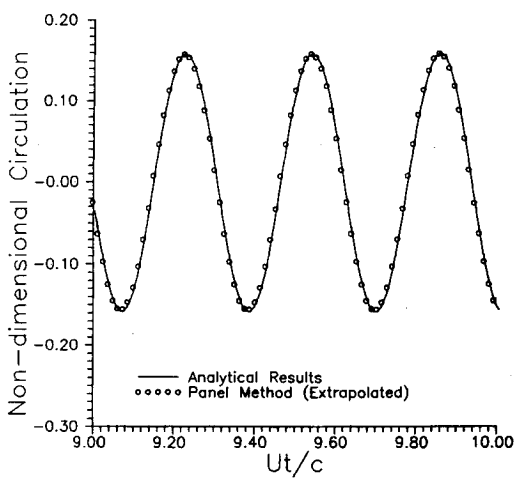

Fig. 8 Consistency test of the present unsteady flow BEM with analytic result. Sinusoidal transverse gust with amplitude $\tilde{v}_g$ = 0.2 and reduced frequency k = 10.

B. Highly Skewed Propeller in Nonuniform Inflow

The unsteady-flow BEM is applied to the highly skewed OBO propeller, of which the discretized geometry is shown in Fig. 9. The geometry of the OBO propeller is given in detail in Ref. 24. The incoming wake is assumed to be axial, U_{Sx}. The harmonic content of U_{Sx} is given in Table 1. The circumferentially averaged U_{Sx} is taken to be invariant in the radial direction and equal to U_P. The advance coefficient, defined as $J_P = 2\pi U_P/(\omega D)$, with D being the diameter of the propeller, is taken equal to 0.727.

The convergence of the results for this case is investigated by varying the chordwise and the spanwise number of panels. To save computing time, a one- (instead of five-) bladed OBO propeller without a hub has been analyzed. The results are shown in terms of the amplitude and phase of the harmonics of the unsteady propeller thrust coefficient, K_T [defined as $K_T(t) = 4\pi^2 T(t)/(\rho\omega^2 D^4)$, with $T(t)$ being the unsteady propeller thrust at time t], at different frequencies (integer multiples of the frequency of propeller rotation) in Figs. 10 and 11. The reduced frequency, $k_{0.7}$ [defined as $k_{0.7} = n_H \omega c/(2\sqrt{U_P^2 + (\omega r)^2})$, with c being the blade chord length at r = 0.7 of the propeller radius and n_H = 1, 2, . . . the harmonic number] is approximately equal to $k_{0.7}$ = 1 at the fifth harmonic and to $k_{0.7}$ = 3 at the 15th harmonic. The thrust includes only the inviscid flow terms as described in Sec. IV. The convergence with respect to all discretization parameters is shown to be very good. In all previous cases 120 time steps per revolution ($\Delta\theta_W$ = 3 deg) have been used. Modifying the number of time steps per revolution to 180 has not affected the force harmonics significantly. However, when using 60 time steps per revolution the 15th harmonic has been found to be inaccurate (50% higher amplitude), simply because of the very coarse time discretization of the period of the 15th harmonic of the inflow (four time steps per period). We have found that in order for all harmonics to be accurately evaluated, the period of the highest harmonic of the inflow must be represented with at least eight time steps. The convergence of the results with number of panels for the OBO propeller in steady flow, when all the blades and the hub are included in the calculations, can be found in Ref. 19. The rate of the convergence does not appear to be affected by the presence of the other blades or the hub, and this has been found to be also true in the case of unsteady flows. In the present work

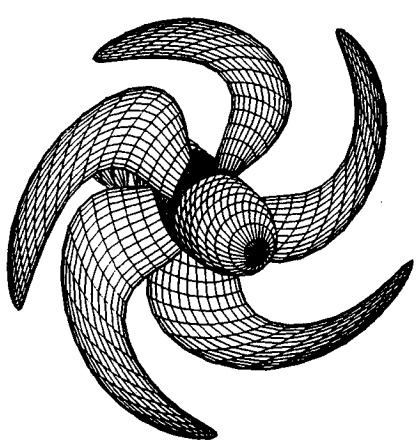

Fig. 9 The geometry of the OBO propeller.

Table 1 Harmonic analysis of the wake inflow

Harmonic	Amplitude	Phase, deg
1	0.1500	0.0
5	0.1000	0.0
10	0.1000	180.0
15	0.1000	180.0

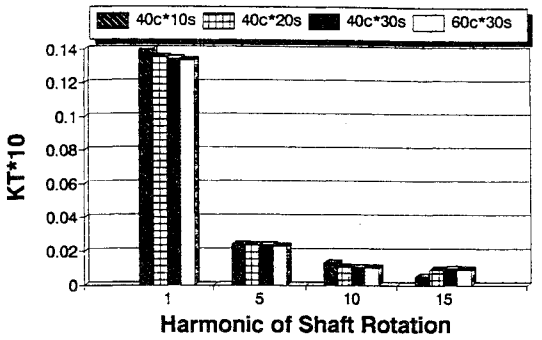

Fig. 10 Amplitude of the unsteady thrust vs harmonic number predicted from the present BEM for the OBO propeller and for various discretizations.

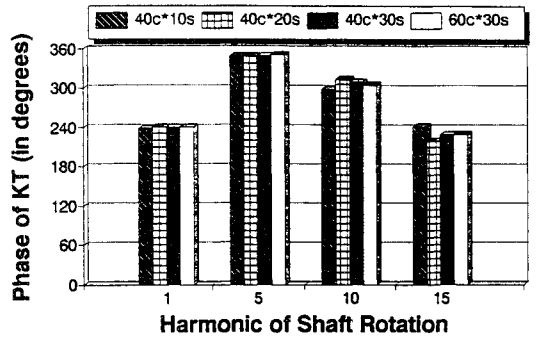

Fig. 11 Phase of the unsteady thrust vs harmonic number predicted from the present BEM for the OBO propeller and for various discretizations.

we chose to show only the convergence of the propeller forces. However, more detailed convergence tests (in terms of the spanwise circulation distribution) for the OBO as well as for other propeller geometries can be found in Refs. 19 and 21. In general, the convergence of the circulation distribution has been found to be faster than that of the forces. Comparisons of the spanwise circulation distribution from the present method and from the BEMs described in Refs. 7 and 9 can be found in Ref. 19 in the case of the OBO propeller in steady flow. Finally, the present method has been shown to satisfy the consistency test vs the (zero thickness) lifting surface method when applied to propellers in steady or unsteady flows as may be found in Refs. 19 and 21.

VI. Harmonic Content of Propeller Forces

From the harmonic analysis of the forces on the OBO propeller, described in the previous section, it is found that nonzero force amplitudes exist for some harmonics different from those of the incoming flow. This is more apparent for the torque coefficient, $K_Q(t)$, harmonics for which the amplitudes are shown in Table 2. The torque coefficient is defined as $K_Q(t) = 4\pi^2 Q(t)/(\rho\omega^2 D^5)$, with $Q(t)$ being the unsteady propeller torque at time t. Those additional harmonics do not go away as the number of panels increase or as the propeller is running through more revolutions in order for the transients to disappear. The results shown in Table 2 were produced with 180 time steps per revolution, at which the values of all the harmonics were found to be converged.

To explain the observed contamination of the harmonic content of the forces, we consider a symmetric NACA66 10% thick section subject to a sinusoidal transverse gust as shown in Fig. 5. For that foil, the normal to the chord, F_y, and the chordwise, F_x, components of the total force (their direction is along the x and y axes shown in Fig. 5) are computed and shown in Fig. 12 as a function of time over one period of the gust. It is apparent from Fig. 12 that the normal force has

Table 2 Amplitudes of torque harmonics for one-bladed OBO propeller

Harmonic	Amp*1000	Harmonic	Amp*1000	Harmonic	Amp*1000
1	1.353	11	0.014	21	0.000
2	0.075	12	0.000	22	0.000
3	0.000	13	0.000	23	0.000
4	0.008	14	0.011	24	0.000
5	0.300	15	0.070	25	0.014
6	0.015	16	0.007	26	0.000
7	0.000	17	0.000	27	0.000
8	0.000	18	0.000	28	0.000
9	0.012	19	0.000	29	0.000
10	0.068	20	0.004	30	0.004

The harmonics that correspond to the frequencies of the inflow are shown underlined.

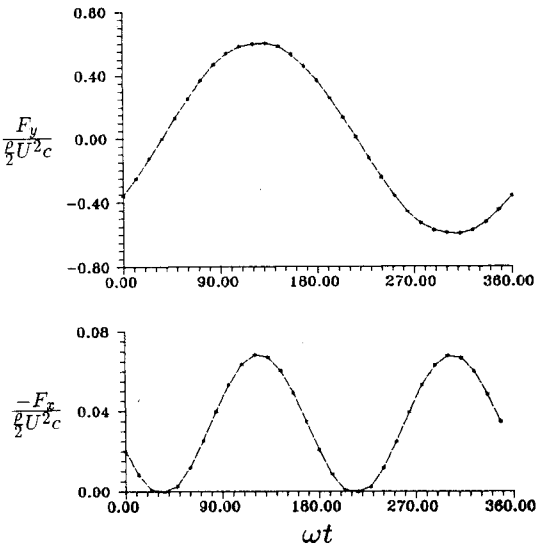

Fig. 12 Normal to the chord, $F_y(t)$, and chordwise force, $F_x(t)$, on a two-dimensional symmetric foil subject to a sinusoidal transverse gust. Same geometry and flow conditions as in Fig. 6.

zero mean and the same frequency as the incoming gust, as opposed to the chordwise force, which has a nonzero mean and a twice as big frequency. This can be explained from the following quasisteady argument. In case the gust, of amplitude $\tilde{v}_g$ and frequency ω, is very slow ($k = \omega c/2U \to 0$), the total force will be normal to the total inflow vector with components along the x and y axes given as

$$F_y = \rho U\Gamma \tag{21}$$

$$F_x = -F_y \frac{v_g}{U} = -\rho v_g \Gamma \tag{22}$$

where Γ is the circulation around the foil, taken as positive in the clockwise direction.

On the other hand, Γ behaves linearly with v_g. This holds for any symmetric foil in potential theory with no assumption made concerning the magnitude of v_g or of the foil thickness. In the case of a flat plate $\Gamma = \pi c v_g$. Therefore, the normal force is linear with v_g and the chordwise force quadratic with v_g. As a result of this, the frequency of the normal force is equal to ω and that of the chordwise force 2ω. It can be shown easily that

$$\bar{F}_x = -\overline{F}_x \to \tilde{F}_y \frac{\tilde{v}_g}{2U} \text{ as } k \to 0 \tag{23}$$

where $\overline{F}_x$ and $\tilde{F}_x$ correspond to the mean and the amplitude of F_x, respectively. The nonzero mean $\overline{F}_x < 0$ is consistent with the well-known fact of hydrofoil propulsion in unsteady

flow. For reduced frequencies $k > 0$, the ratio $\tau = \tilde{F}_x/\tilde{F}_y = f(k)\tilde{v}_g/2U$ depends on k as well as on the geometry of the foil. For example at $k = 0$, $f(k) = 1$ and at $k = 0.5$, shown in Fig. 12, $f(k) = 0.57$.

Due to the quadratic behavior of the chordwise force component with respect to the gust, its harmonic content will correspond to harmonics with frequencies twice as large as those of the incoming flow as well as with frequencies resulting from the sum and difference of the gust frequencies. In the case of a propeller, due to the blade orientation both the normal and chordwise (now perpendicular to the leading-edge line) forces at each blade section will contribute to the propeller thrust or torque. In addition, due to the obliqueness of the incoming gust with respect to each local blade chord, there will also be quadratic in v_g terms contributing to the normal blade force as shown by Brown.[25] Thus, in the harmonic analysis of propeller blade forces, the incoming frequencies, twice as much as these frequencies, and all combinations of the their sums and differences (of the incoming frequencies) should appear. For example, in the case of the one-bladed OBO propeller, the frequencies of the incoming flow were 1, 5, 10, 15 times the fundamental propeller rotation frequency ω. The additional frequencies, shown in Table 2, should thus correspond to the following multiples of ω: $2 = 2 \times 1$, $20 = 2 \times 10$, 30, $4 = 5 - 1$, $6 = 5 + 1$, 9, 11, 14, 16, $25 = 10 + 15$. Notice that in this particular application the amplitudes of the additional frequencies vary from 5% to 20% of the amplitudes at the harmonics of the inflow.

Finally, in the case of the five-bladed OBO propeller the only frequencies that may have nonzero amplitudes for the thrust or torque acting on the shaft should be those corresponding to multiples of $5 \times \omega$, i.e., 5, 10, 15, 20, 25, 30. In this case the frequency contamination corresponds to 20, 25, and 30ω.

The unsteady wake relaxation is also expected to contaminate the inflow frequencies, due to its nonlinear character with respect to the inflow. In the present work, however, the trailing wake geometry is frozen with time, and the contamination of the inflow harmonics is simply due to the nonlinear dependency of the forces with respect to the inflow. In general, the effect of the unsteady wake relaxation on the propeller forces is not expected to be as strong as in the case of helicopter blades for which the pitch is usually much lower than that of the blades of a marine propeller.

VII. Conclusions

A time-marching potential-based BEM was presented for the analysis of the unsteady flow around open marine propellers subject to spatially nonuniform inflows. An efficient algorithm has been implemented in order to ensure an explicit Kutta condition (i.e., pressure equality) at the blade trailing edge at each time step. The numerics of the present BEM when applied to hydrofoils or extreme propeller geometries are shown, here and in the cited references, to be very robust for a broad range of reduced frequencies. the method is also shown to be consistent with known analytic solutions for unsteady flows in two dimensions. The method provides the user with numerically accurate unsteady pressure distributions which may be coupled with a viscous/inviscid interaction scheme to predict unsteady boundary-layer separation and/or leading-edge separation.

Finally, it is shown that the harmonic content of the blade forces should correspond to the frequencies of the incoming flow, twice as much as those frequencies, as well as frequencies resulting from the sum or difference of the incoming frequencies.

Appendix A: Dipole Distribution at First Panel in Wake

Consider a blade strip and its wake (with the index number m being omitted for simplicity) as shown in Fig. 3, and assume a dipole distribution on the first wake panel which is linear along the chordwise direction. The dipole strength, $\mu(s)$, at time step $n = t/\Delta t$ will be given as follows:

$$\mu(s) = \Gamma(n) + \frac{\Gamma(n-1) - \Gamma(n)}{\Delta x_W} s \tag{A1}$$

where Δx_W is the chordwise length of the first wake panel, and s is the chordwise distance from the blade trailing edge. $\Gamma(n)$ and $\Gamma(n-1)$ are the circulations at time steps (n) and $(n-1)$ and, according to Eqs. (5) and (6), they also are the dipole strengths at the "left" and "right" edge of the panel, respectively. The influence, I_P, of the first wake panel at any point P in the flowfield can be expressed in the following integral form:

$$I_P = \int_A w(s, r)\mu(s)\, ds\, dr \tag{A2}$$

where A is the surface of the panel described in terms of the curvilinear orthogonal coordinates s and r, and w is the influence to point P of a unit strength dipole normal to the surface of the panel at location (s, r). by using Eq. (A1) I_P can be expressed as

$$I_P = T^L\Gamma(n) + T^R\Gamma(n-1) \tag{A3}$$

where $\bar{s} = s/\Delta x_W$ and T^L and T^R are defined as follows:

$$T^L = \int_A w(s, r)[1 - \bar{s}]\, ds\, dr$$

$$T^R = \int_A w(s, r)\bar{s}\, ds\, dr \tag{A4}$$

T^L (T^R) corresponds to the influence coefficient, due to a linear dipole distribution (in the chordwise direction) on the first wake panel, whose value is one (zero) at the trailing edge and zero (one) at the other edge. In the case of two-dimensional flows, T^R and T^L can be expressed analytically.[26] In the case of propeller flows, analytical expressions for T^R and T^L can also be found by using similar techniques to those described in Ref. 18.

Appendix B: Details of Unsteady Kutta Condition

Iterative Newton-Raphson Scheme

The pressure difference, Δp_m, at the trailing edge of each blade strip m is defined as

$$\Delta p_m(n) = p_m^+(n) - p_m^-(n) \tag{B1}$$

with p_m^+ and p_m^- being the pressures at the upper and lower trailing edge, respectively.

We call ϕ_j^* and Γ_m^* the potentials and the circulations, respectively, which satisfy Eq. (17) and which, in addition, produce a zero pressure difference (within a desired tolerance) at the blade trailing edge. That is,

$$[A][\phi^*] + [T][\Gamma^*] = [RHS] \tag{B2}$$

and

$$\Delta p_m^*(n) = 0; \qquad m = 1, M \tag{B3}$$

Because of the nonlinear dependence of Δp_m^* on ϕ^*, an iterative method is used in solving the system of Eqs. (B2) and (B3) with respect to the unknown ϕ_j^*s and Γ_m^*s. The following M-dimensional Newton-Raphson scheme is employed in order to determine the circulations Γ_m^*s:

$$[\Gamma^*]^{(k+1)} = [\Gamma^*]^{(k)} - [J^{(k)}]^{-1}[\Delta p^*]^{(k)} \tag{B4}$$

where k denotes the iteration number and $[\Delta p^*]^{(k)}$ are the pressure differences which correspond to the solution $[\phi^*]^{(k)}$ of the system of linear equations

$$[A][\phi^*]^{(k)} = [RHS] - [T][\Gamma^*]^{(k)} \tag{B5}$$

The first iteration ($k = 1$) is taken equal to the solution when the Kutta condition [Eq. (14)] is applied as

$$[\phi^*]^{(1)} = [\phi] \text{ and } [\Gamma^*]^{(1)} = [\Gamma] \tag{B6}$$

In Eq. (B4) the elements of the Jacobian matrix $[J^{(k)}]$ are defined as

$$J_{i,j}^{(k)} = \frac{\partial \Delta p_i^{*(k)}}{\partial \Gamma_j^{*(k)}} \tag{B7}$$

It has been found that the values of $J_{i,j}^{(k)}$ do not change rapidly during the iterations. Thus, their values are computed at the first iteration and then are kept the same throughout the iterative process. This corresponds to the modified Newton-Raphson method. The involved derivatives are computed as follows:

$$J_{i,j}^{(k)} = J_{i,j} = \frac{\partial \Delta p_i}{\partial \Gamma_j} = \frac{\Delta p_i^{\beta} - \Delta p_i^{0}}{\Gamma_j^{\beta} - \Gamma_j^{0}} \tag{B8}$$

where the superscript (0) corresponds to the solution from applying Eq. (14) and the superscript (β) corresponds to the solution where Γ_j^0 is perturbed as follows:

$$\Gamma_j^{\beta} = (1 + \beta)\Gamma_j^0 \tag{B9}$$

where β is a small (positive or negative) number. Even though the results appear not to be sensitive on β, $\beta = 0.01$ has been used. Equation (B4) is finally modified to:

$$[\Gamma^*]^{(k+1)} = [\Gamma^*]^{(k)} - [J]^{-1}[\Delta p^*]^{(k)} \tag{B10}$$

The present iterative scheme has been found to converge rapidly (in three to four iterations). This would require solving, for each time step, the system of equations (B5) as many times as the number of iterations. As a result, the already considerable computing time would be increased approximately by a factor equal to the number of iterations, since a substantial part of the total computing time is devoted in inverting the system of equations (B2). Instead of inverting the system of equations (B5) at each time step, the technique of the base problems has been developed and implemented, as described in the next section.

Base Problems

First, the observation is made that for each time step the matrix $[RHS]$ is identical in Eqs. (B2) and (B5). Thus, subtracting Eq. (B5) from Eq. (B2) we get

$$[A]\left[[\phi^*]^{(k)} - [\phi]\right] = -[T]\left[[\Gamma^*]^{(k)} - [\Gamma]\right] \tag{B11}$$

By defining

$$[\delta\phi] = [\phi^*]^{(k)} - [\phi] \text{ and } [\delta\Gamma] = [\Gamma^*]^{(k)} - [\Gamma] \tag{B12}$$

Eq. (B11) can then be written as

$$[A][\delta\phi] = -[T][\delta\Gamma] \tag{B13}$$

At this point, we define the base potentials, $[\Phi]^m$, which correspond to the system of equations (B13), and which are the solutions to the base problems

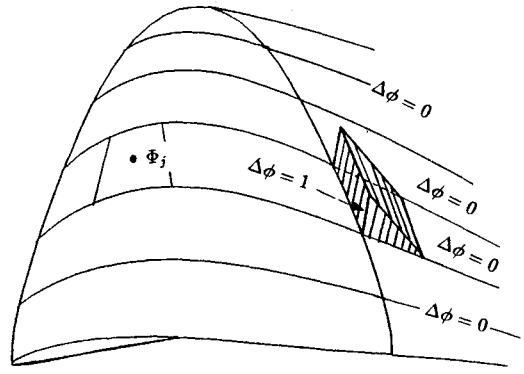

Fig. B1 Definition of the base problem at blade strip m.

$$[A][\Phi]^m = -[T][B]^m, \qquad m = 1, M \tag{B14}$$

where

$$[B]^m = [B_1 = 0, B_2 = 0, \ldots, B_m = 1, \ldots, B_M = 0]^T \tag{B15}$$

Physically, the base potentials $[\Phi]^m$ correspond to the potentials on the propeller blade, when there is no inflow and the potential jumps are equal to zero in all the wake panels except the first panel in the wake at blade strip m, in which there is a linear dipole distribution with potential equal to unity at the left (trailing edge) end, and equal to zero at the right end. The base problem is also shown schematically in Fig. B1. Notice that the base solutions depend only on the propeller discretization and that they are independent of the propeller inflow and the time step n. Due to the linear character of the system of equations (B13), the solution $[\delta\phi]$ can then be expressed as a linear superposition of the base potentials

$$[\delta\phi] = \sum_{m=1}^{M} \delta\Gamma_m[\Phi]^m \tag{B16}$$

and by using the definitions (B12), the solution to the system of equations (B5) is expressed as:

$$[\phi^*]^{(k)} = [\phi] + \sum_{m=1}^{M} (\Gamma_m^{*(k)} - \Gamma_m)\,[\Phi]^m \tag{B17}$$

In conclusion, by employing the previously described technique of the base problems, we avoid solving the system of equations (B5) for each Kutta condition iteration and at each time step. Instead, we express the solution to Eq. (B5) in terms of the base potentials. The base potentials are determined before the unsteady solution process starts, by solving the system of equations (B14) as many times as the number of the spanwise blade sections M, which is far less than the number of times the system of equations (B2) is solved. As a result the increase in the total computing time, when the present iterative pressure Kutta condition is applied, is insignificant.

Acknowledgments

Support for this research was provided by the MIT Sea Grant College Program and the David Taylor Research Center, Department of the Navy, Grant NA86AA-D-SG089, and by the Office of Naval Research Contracts N00014-89-J-3194 and N00014-87-K-0422. The authors would like to thank Justin E. Kerwin of the Department of Ocean Engineering at MIT for his comments and discussions during the course of this work.

References

[1]Hanaoka, T., "Hydrodynamics of an Oscillating Screw Propeller." *Proceedings of the 4th Symposium on Naval Hydrodynamics*, Washington, DC, 1962.

[2]Hanaoka, T., *Numerical Lifting Surface Theory of a Screw Propeller in Non-uniform Flow. Part 1: Fundamental Theory*, Technical Rept. 6(5):1-14, Ship Res. Inst., Tokyo, 1969.

[3]Tsakonas, S., Jacobs, W. R., and Rank, P. H., "Unsteady Propeller Lifting-Surface Theory with Finite Number of Chordwise Modes," *Journal of Ship Research*, Vol. 12, No. 1, 1968, pp. 14–45.

[4]Tsakonas, S., Jacobs, W. R., and Ali, M. R., "An Exact Linear Lifting-Surface Theory for a Marine Propeller in a Nonuniform Flow Field," *Journal of Ship Research*, Vol. 17, No. 4, 1973, pp. 196–207.

[5]Kerwin, J. E., and Lee, C.-S., "Prediction of Steady and Unsteady Marine Propeller Performance by Numerical Lifting-Surface Theory," *Transactions of the Society of Naval Architects and Marine Engineers*, Vol. 86, 1978, pp. 218–253.

[6]Kerwin, J. E., "Marine Propellers," *Annual Review of Fluid Mechanics*, Vol. 18, 1986, pp. 387–403.

[7]Hess, J. L., and Valarezo, W. O., "Calculation of Steady Flow About Propellers by Means of a Surface Panel Method," *23rd Aerospace Sciences Meeting*, AIAA, Reno, NV, Jan. 1985.

[8]Kerwin, J. E., Kinnas, S. A., Lee, J.-T., and Shih, W.-Z., "A Surface Panel Method for the Hydrodynamic Analysis of Ducted Propellers," *Transactions of the Society of Naval Architects and Marine Engineers*, Vol. 95, 1987, pp. 93–122.

[9]Hoshino, T., "Hydrodynamic Analysis of Propellers in Steady Flow Using a Surface Panel Method," *Proceedings of the Spring Meeting*, The Society of Naval Architects of Japan, May 1989.

[10]Hess, J. L., "Calculation of Potential Flow About Arbitrary Three-Dimensional Lifting Bodies," Technical Rept. MDC J5679-01, McDonnell Douglas, Oct. 1972.

[11]Morino, L., and Kuo, C.-C., "Subsonic Potential Aerodynamic for Complex Configurations: a General Theory," *AIAA Journal*, Vol. 12, no.2, 1974, pp. 191–197.

[12]Giesing, J. P., "Nonlinear Two-Dimensional Unsteady Potential Flow with Lift," *Journal of Aircraft*, Vol. 5, No. 2, 1968, pp. 135–143.

[13]Basu, B. C., and Hancock, G. J., "The Unsteady Motion of a Two-Dimensional Aerofoil in Incompressible Inviscid Flow," *Journal of Fluid Mechanics*, Vol. 87, 1978, pp. 159–178.

[14]Maskew, B., "Influence of Rotor Blade Tip Shape on Tip Vortex Shedding—an Unsteady Inviscid Analysis," *Proceedings of 36th Annual AHS Forum*, 1980.

[15]Morino, L., Kaprielian, Z., Jr., and Sipcic, S. R., "Free Wake Aerodynamic Analysis of Helicopter Rotors," Technical Rept. CN. DAAG29-80-C-0016, U.S. Army Res. Office, May 1983.

[16]Greeley, D. S., and Kerwin, J. E., "Numerical Methods for Propeller Design and Analysis in Steady Flow," *Transactions of Society of Naval Architects and Marine Engineers*, Vol. 90, 1982, pp. 415–453.

[17]Lee, J.-T., "A Potential Based Panel Method for The Analysis of Marine Propellers in Steady Flow," PhD Thesis, Dept. of Ocean Engineering, Massachusetts Inst. of Technology, Cambridge, MA, Aug. 1987.

[18]Newman, J. N., "Distributions of Sources and Normal Dipoles over a Quadrilateral Panel," *Journal of Engineering Mathematics*, Vol. 20, 1986, pp. 113–126.

[19]Hsin, C.-Y., "Development and Analysis of Panel Method for Propellers in Unsteady Flow," PhD Thesis, Dept. of Ocean Engineering, Massachusetts Inst. of Technology, Cambridge, MA, Sept. 1990.

[20]Brockett, T., "Minimum Pressure Envelopes for Modified NACA-66 Sections with NACA $a = 0.8$ Camber and Buships Type I and Type II Sections," Rept. 1780, DTNSRDC, Teddington, England, UK, Feb. 1966.

[21]Kinnas, S. A., Hsin, C. Y., and Keenan, D. P., "A Potential Based Panel Method for the Unsteady Flow Around Open and Ducted Propellers," *Proceedings of the Eighteenth Symposium on Naval Hydrodynamics*, Ann Arbor, MI, Aug. 1990.

[22]Sears, W. R., "Some Aspects of Non-stationary Airfoil Theory and Its Practical Application," *Journal of the Aeronautical Sciences*, Vol. 8, No. 2, 1941.

[23]Kinnas, S. A., "A General Theory for the Coupling Between Thickness and Loading for Wings and Propellers," *Journal of Ship Research*, Vol. 36, No. 1, 1992.

[24]Valentine, D. T., and Dashnaw, F. J., "Highly Skewed Propeller for San Clemente Class Ore/Bulk/Oil Carrier Design Considerations, Model and Full-Scale Evaluation," In *First Ship Technology and Research (STAR) Symposium*, The Society of Naval Architects and Marine Engineers, Washington, DC, 1975.

[25]Brown, N. A., "The Periodic Forces Acting on a Propeller Operating in a Circumferentially Non-uniform Inflow," Technical Rept., Dept. of Ocean Engineering, Massachusetts Inst. of Technology, Cambridge, MA, Nov. 1962.

[26]Moran, J., *An Introduction to Theoretical and Computational Aerodynamics*, Wiley, New York, 1984.